Appl Biochem Biotechnol (2011) 165:109–122
DOI 10.1007/s12010-011-9237-8

The Binding of Hepatitis B Virus X Protein to Glioma-Associated Oncogene Homologue 1 and its Biological Characterization In vitro

Bo Bae Jo · Mi Suk Jeong · So Young Park · JaeHun Cheong · Se Bok Jang

Received: 22 October 2010 / Accepted: 28 March 2011 /
Published online: 6 April 2011

Abstract Hepatitis B virus (HBV) X protein (HBx) is a 17-kDa transcriptional coactivator that plays a significant role in the regulation of genes involved in inflammation and cell survival. It has been known to be involved in the development of liver cancer and alteration of the cellular HBx level may influence the pathogenesis of HBV-induced liver diseases. The transcription factor GLI1, a member of the glioma-associated oncogene homologue (GLI) subfamily of Krüppel-like zinc finger proteins is involved in signal transduction within the hedgehog (Hh) signaling pathway, which is involved in the development of many human malignancies. GLI activation is important for cell proliferation and anti-apoptosis in various cancers. To investigate whether the transcriptional coactivator HBx binds to the zinc finger transcription factor GLI1, recombinant HBx and GLI1 were isolated. Expression and purification of the HBx and GLI1 proteins were successfully performed in *Escherichia coli*. The binding of HBx to GLI1 was detected by surface plasmon resonance spectroscopy (BIAcore), fluorescence measurement, and a His-tagged pull-down experiment. After measuring the fluorescence emission spectra of purified HBx and GLI1, it was found that the interaction of these proteins is accompanied by significant conformational changes in one or both. This study provides important clues for the structural identification of signal transduction pathways involving the HBx and GLI1 proteins.

Keywords HBx · GLI1 · Interaction · Hepatocellular carcinogenesis

Introduction

Hepatitis B virus X protein (HBx) has long been suspected to play a positive role in hepatocarcinogenesis because hepatocellular carcinoma (HCC) incidence has been reported in animals infected with mammalian hepadnaviruses [1–3]. Among the proteins encoded by the hepatitis B virus (HBV) genome, a 17-kDa X protein has been shown to be associated

B. B. Jo · M. S. Jeong · S. Y. Park · J. Cheong · S. B. Jang (✉)
Department of Molecular Biology, College of Natural Sciences, Pusan National University, Jangjeon-dong, Geumjeong-gu, Busan 609-735, South Korea
e-mail: sbjang@pusan.ac.kr

with liver carcinogenesis. Expression of the transfected X gene induces transformation of some cell types and induces liver cancer in some transgenic mice [4–7]. However, X transgenes exhibit no obvious pathology in different genetic contexts because of the low level of X protein expression, although these nonpathogenic transgenes cause an increased susceptibility to chemical carcinogenesis [8–10]. It has been shown that X protein facilitates the induction of DNA damage and cell death by localization to the mitochondria [11–14].

Glioma-associated oncogene homologue (GLI) proteins are the effectors of Hedgehog (Hh) signaling and have been shown to be involved in cell fate determination, proliferation, and patterning in many cell types and most organs during embryo development [15]. GLI transcription factors activate/inhibit transcription by binding to GLI-responsive genes and by interacting with the transcription complex. GLI transcription factors have DNA-binding zinc finger domains, which bind to consensus sequences on their target genes to initiate or suppress transcription [16]. Liu et. al. [17] showed that mutating the GLI zinc finger domain inhibits the proteins' effect, proving its role as a transcription factor. GLI proteins have an 18-amino acid region highly similar to the α-helical herpes simplex viral protein 16 activation domain. This domain contains a consensus recognition element for the human TFIID TATA box-binding protein associated factor TAFII31. Missing in metastasis (MIM/BEG4) has been shown to potentiate the effects of GLI transcription factors on target gene transcription. GLI and MIM have been shown to act synergistically to induce epidermal growth, and MIM+ GLI1 overexpressing grafts show similar growth patterns to Sonic hedgehog (Shh) grafts [18].

HBx is a multifunctional regulator that modulates transcription, signal transduction, cell cycle progress, protein degradation pathways, apoptosis, and genetic stability by directly or indirectly interacting with host factors. In light of the evidence suggesting that the X protein has a transactivation function, a recent study showed that HBx has a putative nucleic-acid binding motif such as the zinc finger structure. Surprisingly, four conserved cysteine residues positioned at 7, 17, 61, and 69 that might form a structure similar to the zinc finger motif were found in all X gene sequences [19]. GLI1 encodes a nuclear protein, containing five zinc finger motifs, which bind to DNA in a sequence-specific manner [20,21]. We isolated and purified recombinant HBx and GLI1, and we showed through a series of biochemical and biophysical measurements that HBx interacts with GLI1 in vitro. This study provides important clues for the structural identification of signal transduction pathways involving the HBx and GLI1 proteins.

Materials and Methods

Cloning of HBx and GLI1

To determine the soluble and overexpressed regions of HBx and GLI1, the cloning of four fragments were conducted as follows.

HBx (1–50), 5′-CGGAATTCATGGCTGCTAGGCTGTGCT-3′ (forward) and 5′-CCGCTCGAGTTACCCGTGGTCGGCCGGAA-3′ (reverse);
HBx (51–154), 5′-CGGAATTCATGGCGCACCTCTCTTTACG-3′ (forward) and 5′-CCGCTCGAGTTAGGCAGAGGGGAAAAAGTT-3′ (reverse);
HBx (full-length, 1–154), 5′-GGAATTCCATATGGCGCACCTCTCTTTACG-3′ (forward) and 5′-CGCGGATCCTTAGCATGGTGCTGGTGAACA-3′ (reverse);
GLI1 (230–390), 5′-GGAATTCCATATGGAATCTGTGTATGAAAC-3′ (forward) and 5′-CCGCTCGAGGTCAGGACCATGCAC-3′ (reverse).

Truncated HBx proteins (1–50 and 51–154) were amplified by PCR using oligonucleotides incorporating *Eco*RI and *Xho*I sites in the 5′ primer and 3′ primer containing a stop codon. The GLI1 construct corresponding to amino acids 230–390 of the full-length human GLI1 (1–1106) protein was amplified by PCR using oligonucleotides incorporating *Nde*I and *Xho*I sites in the 5′ primer and 3′ primer containing a stop codon. The amplifications of HBx and GLI1 were performed using a procedure of 30 cycles of reaction with denaturing at 94°C for 1 min, annealing at 53°C for 30 s, and extension at 72°C for 1 min. After digestion, the HBx fragments were inserted into the GST-fusion expression vector pGEX-4T-1 and were linked by T4 ligase, producing a recombinant vector pGEX-4T-1-HBx. After the GLI1 fragment was digested, it was incorporated into the plasmid pET-26b (Novagen) with strong T7 transcriptional and translational sequences. The positive GST–HBx and His-GLI1 fusion expression plasmids were identified by restriction endonuclease digestion and further verified by DNA sequencing, using a Macrogen automatic DNA sequencer.

Expression Conditions

The HBx and GLI1 constructs were transformed into the expression host *Escherichia coli* BL21(DE3). A single colony was inoculated with 5 mL of Luria–Bertani (LB) medium containing 50 μg/mL ampicillin. Bacteria were grown overnight at 37°C. The cells were added to inoculate 500 mL of LB with antibiotics. The cultures were grown at 37°C until OD_{600} reached 0.5. The expression of the protein was induced with 0.5 mM of isopropyl-thio-β-D-galactopyranoside. The bacterial cells were induced for 4–6 h at 37°C and then harvested by centrifugation at 4,500 rpm for 20 min. The cell pellets were either immediately used or stored frozen at −70°C. The HBx cells were collected by centrifugation for 40 min at 4°C and resuspended in PBS buffer [4.3 mM Na_2HPO_4, 1.47 mM KH_2PO_4, 137 mM NaCl, and 2.7 mM KCl (pH 7.3)]. The GLI1 cells were collected by centrifugation for 45 min at 4°C, followed by resuspension in buffer A [50 mM Tris–HCl (pH 7.5), and 200 mM NaCl], after which they were disrupted by sonication on ice. Subsequently, the cell debris was discarded by 45 min of centrifugation at 14,500 rpm. The whole cells and soluble and insoluble fractions were fractionated on 12% SDS-PAGE gels and visualized by Coomassie blue staining.

Purification of HBx and GLI1

The clear HBx (1–50) supernatant was loaded onto the glutathione-Sepharose four fast flow (Amersham-Pharmacia Biotech; binding capacity 10 mg GST per milliliter of resin) at a flow rate of 2.5 mL/min and washed extensively with 20 mL of PBS buffer. The GST–HBx fusion protein was eluted with 10 mL of 10 mM reduced glutathione dissolved in 50 mM Tris–HCl. The eluted fraction was dialyzed against elution buffer for 12 h at 4°C. The reaction mixture was loaded at 2.5 mL/min to a Q-Sepharose fast-flow (Amersham-Pharmacia Biotech) anion exchange chromatography column pre-equilibrated with buffer B [50 mM Tris–HCl (pH 7.5), 200 mM NaCl, and 1 mM DTT]. Elution was performed with the salt gradient of the NaCl solution. The protein was passed through the Q-Sepharose column to remove cellular DNA and negatively charged acidic protein. The HBx protein was concentrated by centrifuging it at 2,500 rpm using ultrafiltration devices, to a final volume of 10 mL. Successively, gel filtration was performed using a Superdex 75 HPLC column (Fig. 2a).

To obtain soluble proteins of insoluble fractions HBx (51–154 and full-length), refolding processes were performed. The inclusion bodies of GST–HBx were resuspended under protein denaturing conditions in buffer B containing 6 M urea. The resuspended cells were

then centrifuged at 14,500 rpm for 45 min at 4°C in a refrigerated high speed centrifuge. The supernatant was collected and loaded onto a column containing 7 mL pre-equilibrated GST resin. The loaded protein was refolded by gradient against buffer B and then eluted with buffer B containing 10 mM reduced glutathione. The eluted fractions were dialyzed against buffer B to remove the glutathione.

Clear GLI1 supernatant was loaded onto a Ni-NTA (Amersham-Pharmacia Biotech) column and pre-equilibrated with buffer A. The column was washed with buffer A containing 20 mM imidazole at a flow rate of 2.5 mL/min, and bound protein was then eluted using concentrations of imidazole varying from 20 to 200 mM. Gel filtration was performed by HPLC using a Superdex 200 HR10/30 column (Amersham-Pharmacia Biotech) equilibrated in buffer A. HBx and GLI1 were separated, and the fractions were collected and concentrated to final volumes of 1 mL. The protein solutions were concentrated to 1–2 mg/mL using a Vivaspin 20 (Sartorius).

Western Blotting

The purified GLI1 protein from SDS-PAGE (12%) was transferred onto a nitrocellulose membrane at 115 V for 1 h. The membrane was blocked with 5% skim milk in Tween-PBS buffer containing 1% Tween 20 for 2 h. The membrane was then incubated in the primary antibody [His-probe (G-18) diluted 1:1,000] for 12 h. After washing with Tween-PBS, the membrane was incubated for 1 h with goat anti-rabbit IgG-HRP (Santa Cruz Biotechnology, Inc.) secondary antibody diluted at a ratio of 1:10,000 in blocking buffer.

His-Tagged Pull-Down Assay

For the pull-down experiment, His-tagged fusion protein-immobilized sepharose beads were prepared. A total of 50 μg each of purified HBx and His-tagged GLI1 was mixed with 50 μL Ni-metal chelating affinity resin in binding buffer B by rotating at 4°C for 3 h. The supernatant was removed by centrifugation at 8,000 rpm for 3 min. The beads were then washed three times with buffer B. Each time, the beads were incubated with wash buffer on a rotator for 3 min and collected by centrifugation. The beads were eluted with elution buffer B containing 200 mM imidazole, boiled in SDS sample loading buffer for 5 min, and then resolved by SDS-PAGE for Coomassie blue staining.

Far-UV Circular Dichroism Spectroscopy Analysis

Circular dichroism (CD) spectropolarimeter (JASCO J-715) measurements using a 0.1-cm cell were carried out at 0.2-nm intervals and at 25°C. The CD spectra of purified recombinant HBx (the average of 10 scans) were recorded in the 190–260 nm range. Far-UV CD spectra were taken at protein concentrations of 0.5 mg/mL. Thermal unfolding was performed using the same set-up by heating the samples with a constant temperature gradient from 4°C to 75°C. The spectra were obtained in milli-degrees and converted to molar ellipticity prior to secondary structural analysis. Calculation of secondary structural elements was performed using the CDNN program.

Inductively Coupled Plasma-Optical Emission Spectrometry

Inductively coupled plasma-optical emission spectrometry (ICP-OES) experiment was performed using a PerkinElmer Model Optima 73000 DV inductively coupled plasma-

optical emission spectrometer (Dual View ICP-OES) with axial (AX-ICP-OES) and radial configurations (RD-ICP-OES) (PerkinElmer Life and Analytical Sciences, Shelton, CT, USA). The instrument has a 40-MHz radio frequency source providing 0.75–1.5 kW of power and utilizes an Echelle grating (79 lines nm^{-1}), a solid-state detector, a plasma torch with a 2.0-mm internal diameter injection tube, and a cross-flow nebulizer coupled with a double-pass Scott-type spray chamber. The equipment also includes an interface (shear gas) that introduces high air perpendicular to the torch, in order to remove the low-temperature extremity of the plasma. The sample introduction system was automated using a Perkin Elmer Model 90 Plus autosampler.

Differential Scanning Calorimetry

Differential scanning calorimetric (DSC) measurements were carried out on a DSC 204F1 (NETZSCH DSC, USA). About 1 mg protein was placed in an aluminum pan, which was then immediately sealed. The pan was heated to −10–90°C at a rate of 1°C/min. An empty pan was employed used as a reference. The sensitivity was 0.1 μw and the sensor time constant was 0.6. The reference was of the same state (liquid) and was placed in a reference crucible made of aluminum. The onset temperature (Tm), peak transition or denaturation temperature (Td), enthalpy of denaturation (ΔH), and cooperativity, as represented by the width at half-peak height (ΔT1/2), were computed from the thermograms using Universal Analysis Version 3.0.3. The sample was examined twice by repeating the heating–cooling cycles. The sealed pan containing protein sample and reference was equilibrated.

BIAcore Biosensor Analysis

Measurements of the apparent dissociation constants (K_D) between HBx (1–50) and GLI1 were carried out using a BIAcore 2000 biosensor (Biosensor, Sweden). HBx [500 μg/mL in 10 mM sodium acetate (pH 5.0)] was covalently bound to the carboxylated dextran matrix at a concentration corresponding to −1,200 response units (RU) by amine-coupling method, as suggested by the manufacturer. A flow path involving two cells was employed to simultaneously measure the kinetic parameters from one flow cell containing the HBx-immobilized sensor chip to the other flow cell containing an underivatized chip. For kinetic measurements at room temperature, GLI1 samples ranging in concentration from 20 to 319 nM were prepared by dilution in HBS buffer [150 mM NaCl, 3 mM EDTA, 0.005% surfactant P20, and 10 mM HEPES (pH 7.4)]. Each sample was injected with 50 μL of GLI1 solution into the flow cells (association phase) at a rate of 10 μL/min. Among the cycles, the immobilized ligand was regenerated by injection with 30 μL of 50 mM NaOH at a rate 10 μL/min.

Fluorescence Spectroscopy

Fluorescence emission spectra were obtained using an Edinburgh (UK) FLS920 TCSPC (Time Correlated Single Photon Counting Spectrometer) with 1-cm path length cuvettes containing excitation and emission slits, 20 nm in width. The fluorescence emission spectra of HBx and GLI1 were obtained in order to identify characteristic chemical structures, namely, double bonds and aromatic groups. The emission intensity was recorded from 300 to 430 nm, with an excitation wavelength of 295 nm. HBx and GLI1 were preincubated together for 25 min at 24°C. The concentration of each protein was 5 μM. All spectra were obtained at a protein concentration 50 μg/mL at 24°C. Ten spectra of each protein sample were accumulated, averaged, and subjected to baseline correction by subtracting the buffer spectrum.

Results and Discussion

HBx is a 154-amino acid protein with an N-terminal negative regulatory domain, a mitochondrial targeting sequence, and a C-terminal transactivation or coactivation domain that has been detected both in the cytoplasm and in the nuclei of infected hepatocytes (Fig. 1a). Neither HBx nor truncated HBx has been expressed in *E. coli* in the soluble form. Up to 52% of the amino acids in the HBx protein are hydrophobic, and the protein contains four disulfide bonds in a unique arrangement [22]. These structural characteristics may increase the HBx protein's tendency for intermolecular aggregation and improper folding and accumulation in the inclusion body fraction. We successfully expressed a high level of GST-fused N-terminal HBx (aa 1–50) in *E. coli* (Fig. 2a). Overexpressed GST-fused HBx (aa 1–50) was identified in the supernatant of a large-scale culture and expressed as a 33-kDa molecule. However, full-length GST-fused HBx (aa 1–154) and truncated HBx (aa 51–154) were overexpressed in the insoluble form and used as a pellet in purification. To obtain soluble and stable forms of these proteins, refolding processes were performed. Both purified full-length HBx and truncated HBx (51–154) showed a homogeneous single band in the SDS-PAGE analysis (Fig. 2a). We successively obtained soluble proteins to final concentrations of 0.5 mg/mL for HBx (1–154) and 1–2 mg/mL for HBx (1–50) and HBx (51–154) using a quantification kit with bovine serum. The secondary structure of HBx was predicted, and HBx was found to possess three alpha-helix, six beta-strands, and loops (Fig. 1c). In the secondary structure of HBx, there is a long loop in the N-terminal region. The long loop region is often flexible and can adopt several different conformations. It induces significant structural disruption and exposure of hydrophobic amino acids, causing aggregation.

Three members of the GLI subfamily GLI1, GLI2, and GLI3 are all transcription factors mediating the Hh pathway. The GLI1, GLI2, and GLI3 genes encode transcription factors, all of which contain conserved tandem CCHH zinc finger domains and a consensus histidine/cysteine linker sequence between zinc fingers (Fig. 1b). The open reading frame encodes a 1,106-amino acid protein, with an estimated molecular weight of approximately 118 kDa. Truncated GLI1 (aa 230–390) protein, including five CCHH zinc finger domains, was expressed mainly in soluble form at 25°C in *E. coli* BL21(DE3) (Fig. 2a). Isolated GLI1 has observed molecular weights of approximately 22 kDa. We obtained a soluble protein with a final concentration of 2 mg/mL for GLI1. The soluble GLI1 protein was purified to homogeneity, and its identity was determined by Western blot analysis (Fig. 2b). The identities of the HBx and GLI1 proteins were determined by MALDI-MS (data not shown). Mass fingerprinting analysis was carried out by subjecting the protein to trypsin digestion. The monoisotopic masses obtained for the individual peptides were in the range of 800–3,000 Da. The sequences of the digested peptides (pI 8.6; molecular weight, 17 kDa for HBx and pI 8.8; molecular weight, 19 kDa for the GLI1) were matched with protein sequences in the database using the PROFOUND program.

GLI1 contains five conserved CCHH zinc finger motifs that coordinate with zinc ions. We confirmed that the intensity of zinc absorption of the GLI1 protein was measured at 206 nm, using inductively coupled plasma-optical emission spectrometry. The content of zinc ions was calculated to be approximately 1.1 M per protein mole. Although zinc ion was detected in small amounts in this protein, it might yet play a role in stabilizing GLI1.

The folding property of the HBx (1–50) protein was characterized by CD spectroscopy. To study the effects of pH on the CD spectra of HBx, the protein was observed under various pH conditions (pH 5.5–9.5) (Fig. 3a). These results show that the CD curve at pH 5.5 was the lowest negative peak and the peak at pH 9.5 was next low negative one.

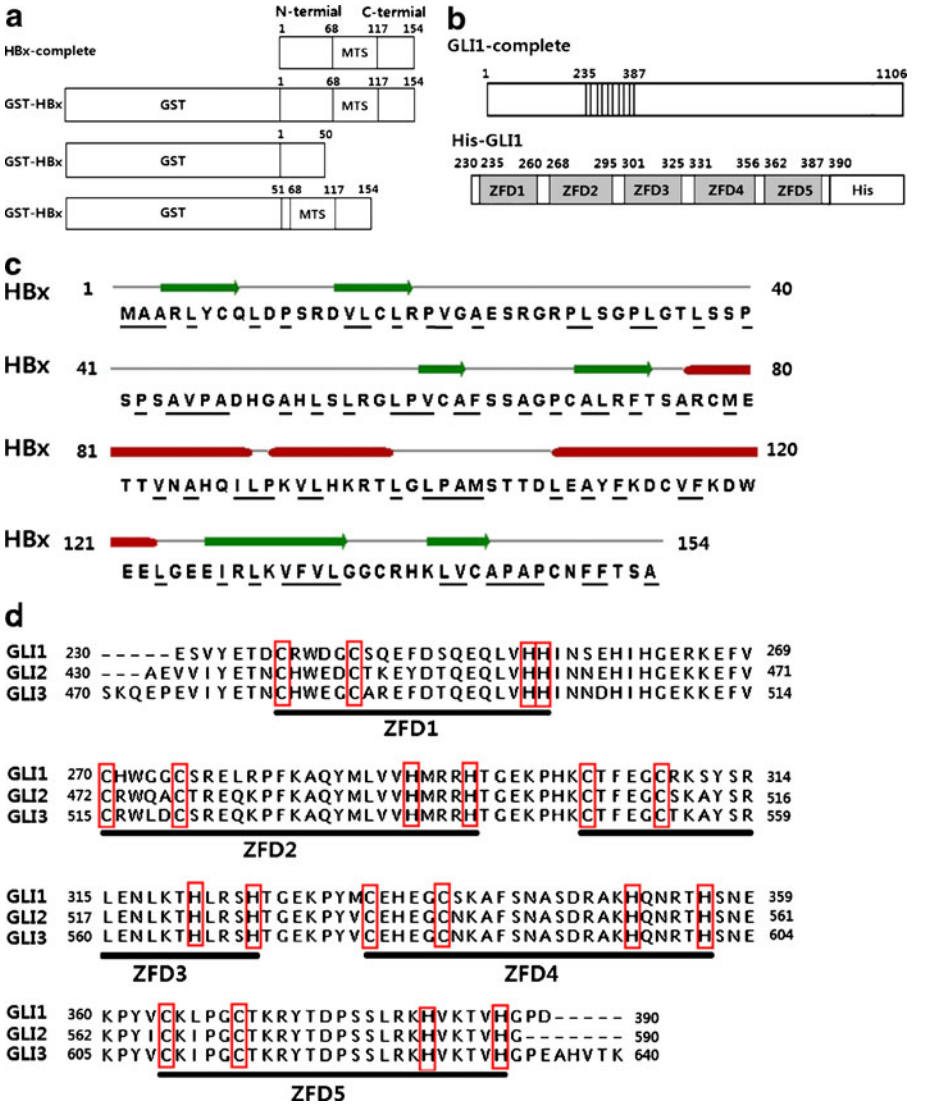

Fig. 1 Deletion constructs of HBx, domain structure of GLI1, sequence alignment of the GLI family, and predicted secondary structure of HBx. **a** Representation of the three different GST–HBx fusion constructs. **b** GLI1 comprises five zinc finger domains. **c** The secondary structure of full-length HBx was predicted. Alpha helices are shown as *red ellipses*, and β-sheets as *green arrows*. Loops are shown as *gray lines*. The hydrophobic residues are indicated by *bars*. **d** Sequence alignments of the GLI family. GLI1 shows high sequence similarity to GLI2 and GLI3. The sequences were aligned using Jalview. The five CCHH zinc finger motifs are indicated by *red boxes*, and the sequences of the motifs in GLI1, GLI2, and GLI3 are also shown

HBx structures between pH 6.5 and pH 8.5 were composed of highly alpha-helical structures. At pH 7.5, the CD spectrum of purified HBx typically exhibited two negative maxima at 210 and 220 nm. Deconvolution of the spectra using the CDNN program indicated the following secondary structure contents for folded HBx, 32.9% α-helices, 19.8% β-sheets, 17.9% turns, and 29.4% non-ordered forms. HBx structure is strongly

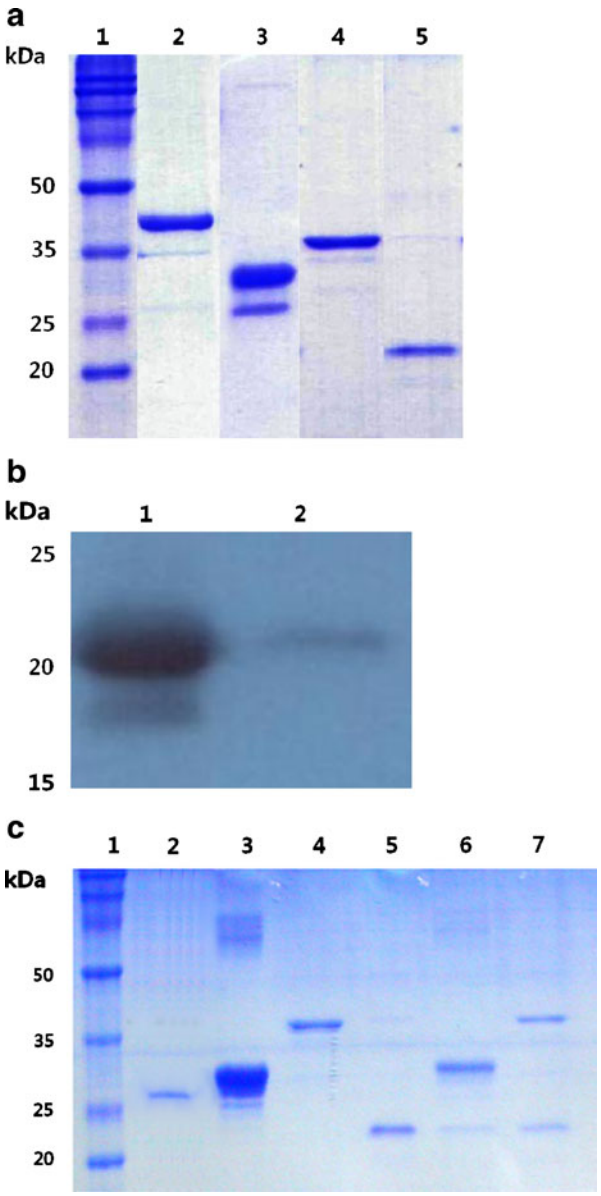

Fig. 2 **a** Purified HBx and GLI1 are subjected to 12% SDS-PAGE. *Lane 1* molecular marker, *lane 2* full-length HBx, *lane 3* HBx (1–50), *lane 4* HBx (51–154), *lane 5* GLI1 (230–390). **b** Western blot analysis of GLI1. *Lane 1* inclusion body, *lane 2* soluble protein. **c** Results of His-tagged pull-down assay using GST–HBx and His–GLI1 in vitro. *Lane 1* molecular marker, *lane 2* GST, *lane 3* HBx (1–50), *lane 4* HBx (51–154), *lane 5* GLI1 (230–390), *lane 6* HBx (1–50)–GLI1 complex, *lane 7* HBx (51–154)–GLI1 complex

dependent on the solution conditions. As such, pH changes induce protonation–deprotonation of dissociable groups of proteins, including the carboxylic acid (aspartic acid and glutamic acid) and amine (lysine, arginine, and histidine) side groups. Due to changes in charge density, the electrokinetic properties of the proteins also varied with pH.

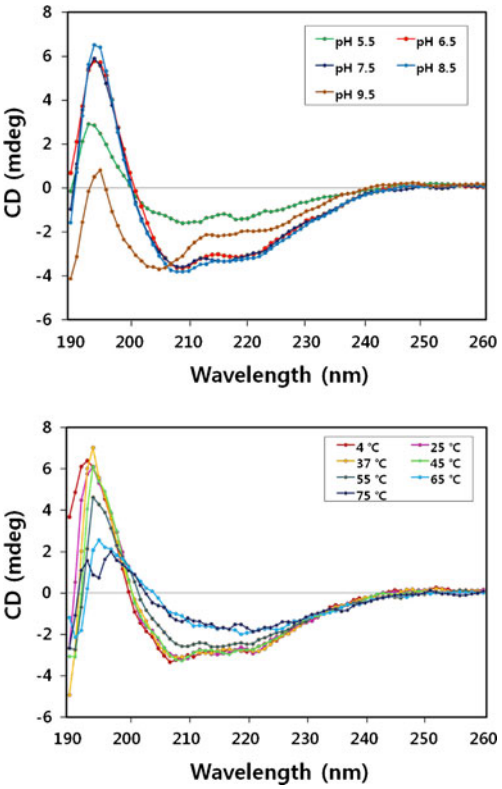

Fig. 3 **a** Far-UV CD spectra of HBx. The experiment was carried out using a JASCO J-715 spectropolarimeter with a 0.1-cm cell at 0.2-nm intervals and 25°C. These spectra were the result of ten scans. CD spectra changes of HBx (1–50) at pH 5.5–9.5 are shown. **b** CD spectra of the HBx protein at different temperatures (4–75°C)

Therefore, an unfolded state corresponding to an extremely low pH and high was observed if all of the ionizable side chains in HBx become fully protonated or deprotonated. The CD spectra of HBx show that pH affected the conformational changes of the proteins to varying extents. Exposing the protein to pH 5.5 and 9.5 significantly changed the conformations of the α-helices, β-sheets, and random coils. The CD spectrum at pH 7.5, except for its negative peak depth, resembled those of the pH 6.5 and 8.5 spectra. These pH-dependent changes in the secondary structures of the proteins can be due to either local structural perturbation or an increased amount of unfolded protein in solution.

Temperature controller spectra were taken at a protein concentration of 1% (*w*/*v*). Thermal unfolding was performed using the same set-up by heating the HBx protein with a constant temperature gradient from 4°C to 75°C (Fig. 3b). An interesting point is that the spectra show more α-helical characteristic bands at low temperatures. Heating caused progressive unfolding of the protein, loss of α-helix, and appearance of characteristic β-sheets. With a gradual increase in temperature, the occurrence of random coils and general characteristics of disordered or loosely folded protein was increased. HBx protein showed significant conformational changes upon temperature changes. Differential scanning calorimetry (DSC) was used to analyze the effects of heat on protein stability. DSC scans were performed for conditions under which the protein was irreversibly unfolded. In this

study, the protein showed thermal transitions or denaturation from −10°C up to 90°C. HBx (1–50) and HBx (51–154) showed an endothermic peak of temperature (T_d) at 46.1°C and 47.7°C, respectively, but GLI1 showed higher endothermic peak at 59.1°C (Fig. 4a).

We showed that HBx interacted with GLI1 in vitro by a series of biochemical and biophysical measurements. The purified HBx and GLI1 proteins were mixed in a 1:1 molar ratio. We confirmed the interaction between HBx and GLI1 by His-tagged pull-down assay (Fig. 2c). To further investigate the interaction between HBx and GLI1, the binding affinity of HBx for GLI1 was estimated by surface plasmon resonance spectroscopy (BIAcore) (Fig. 4b and Table 1). Sensorgrams of HBx binding to GLI1 were used to calculate kinetic binding constants. Background sensorgrams were then subtracted from the experimental ones to yield representative specific binding constants. We found that HBx indeed bound to GLI1 with an apparent K_D of 17 nM. The fluorescence emission spectra of purified HBx and GLI1 were used to confirm their interaction. The λ_{max} curve was found at 330 nm (Fig. 5a, b). The spectrum of the HBx (1–50)–GLI1 (230–390) complex was a little lower than that of HBx (1–50) alone. On the other hand, the spectrum of the HBx (51–154)–GLI1 (230–390) complex was a little higher than that of HBx (51–154) alone. Simply combining the spectra of HBx and GLI1 does not yield the spectra of the HBx–GLI1 complex. The fluorescence intensities were about 7,500 N for GLI1, 7,000 N for HBx (1–50), and

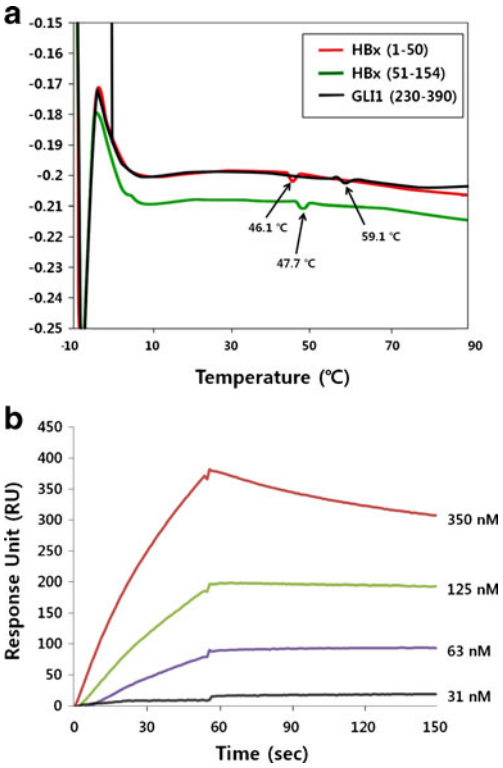

Fig. 4 **a** DSC data spectra of HBx (1–50), HBx (51–154), and GLI1 (230–390). The measurements were carried out a DSC 204F1 (NETZSCH DSC, USA) with the buffer B. HBx (1–50): an endothermic peak of temperature (T_d) at 46.1°C. HBx (51–154): T_d at 47.7°C. GLI1 (230–390): T_d at 59.1°C. **b** BIAcore biosensor analysis of HBx binding to GLI1 at 25°C. The sensorgrams for 31, 63, 125, and 350 nM human GLI1 are shown

Table 1 Kinetic parameters of binding of HBx to GLI1

Concs of analyte (nM)	k_a (M^{-1} s^{-1})	k_d (s^{-1})	K_D (M)
350	3.89×10^{2}	1.31×10^{-3}	3.37×10^{-6}
125	1.35×10^{3}	4.29×10^{-4}	3.19×10^{-7}
63	1.90×10^{3}	3.24×10^{-4}	1.71×10^{-7}
31	8.11×10^{2}	2.31×10^{-3}	2.85×10^{-6}
K_D $(nM)_{avg}$			17

[a] The association rate constant (k_a) was determined from a plot of In[Abs(dR/dt)] versus time, where R is the intensity of the surface plasmon resonance signal at time t. The dissociation rate constant (k_d) was determined from a plot of In(R_o/R) versus time, where R_o is the resonance signal intensity at time zero. The apparent K_D was calculated from the kinetic constants K_D (M)=k_d/k_a

3,500 N for HBx (51–154). The interaction is most likely accompanied by significant conformational changes in either one or both proteins and is likely facilitated since the residues of aromatic groups are buried within the three-dimensional protein structure.

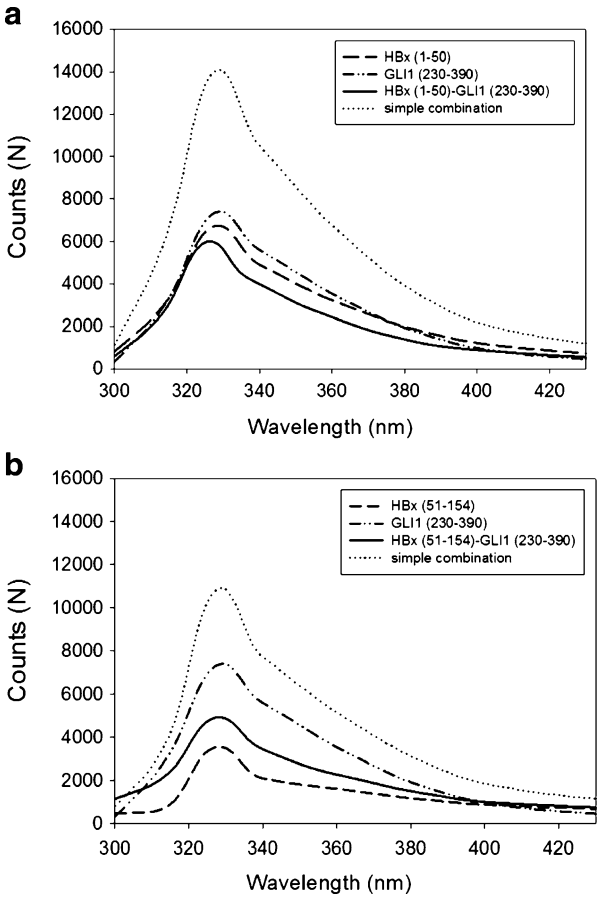

Fig. 5 **a**, **b** Fluorescence analyses of HBx binding to GLI1. Fluorescence spectra of the HBx–GLI1 complex and of each individual protein are shown

Further, the less rigid, hydrophobic environment required for the conformational changes of HBx and GLI1 can be initiated by a decrease in fluorescence intensity. The homology residues for critical interaction between HBx truncations and GLI1 were predicted in Fig. 6a, b. The residues can make a contribution to specific interaction between HBx and GLI1 proteins. Hydrophobic amino acids (L315, L322, and L366) in the GLI1 could be interacted with the hydrophobic amino acids in the HBx (Fig. 6c). The homology residues are located at a structurally important site, situated in a hydrophobic environment. This study has potential applications in medicine and other fields such as mutational study and disease prediction.

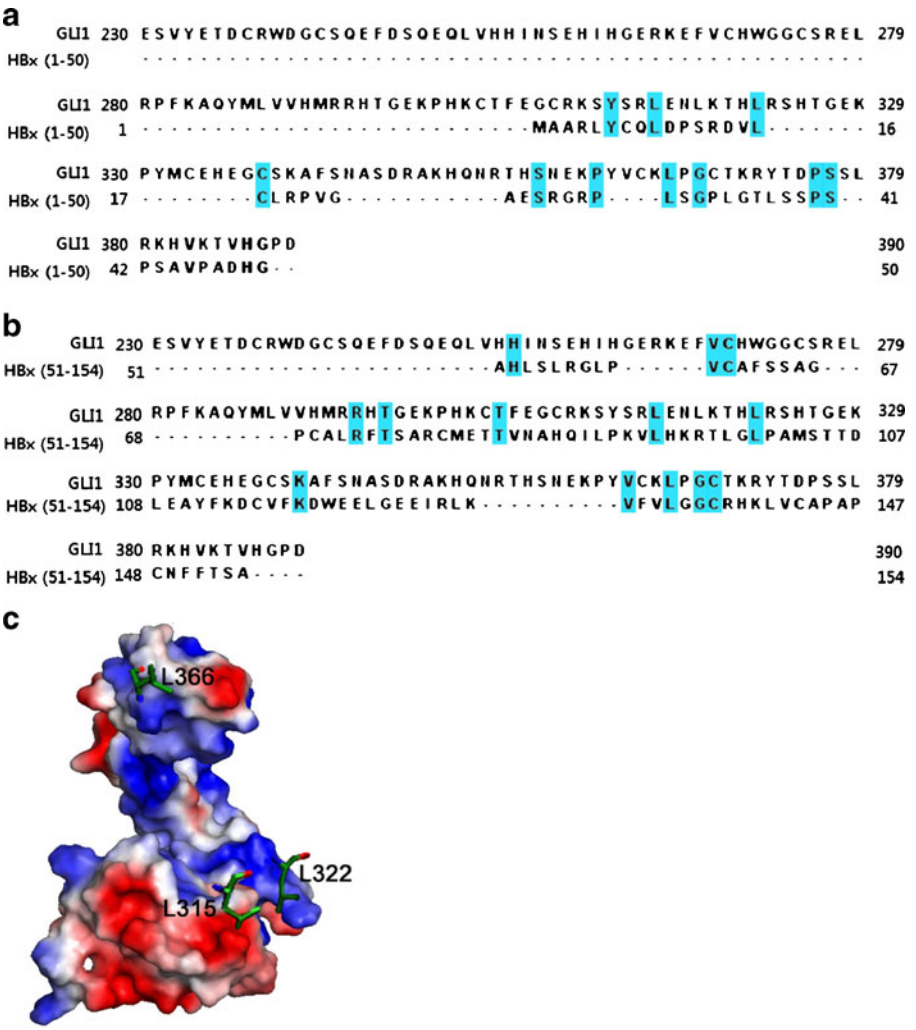

Fig. 6 **a**, **b** The amino acid sequences of the GLI1 protein were compared with those of HBx truncations. The residues conserved in the two species are colored *cyan*, respectively. **c** Surface representation of the GLI1. The predicted homology residues of GLI1 in interactions with the HBx are shown in *black letters*. The relative distribution of surface charge is shown with acidic regions in *red*, basic regions in *blue*, and neutral regions in *white*

In the present study, to identify the interaction and structural integrity of HBx, various biochemical and biophysical techniques, including CD, ICP-OES, DSC BIAcore, and fluorescence were employed. The results provided biological and conformational information on HBx. The results also suggest that the conformations of HBx are, to a certain extent, pH-dependent and temperature-dependent. From the CD and computer predictions of the secondary structures, we conjecture that the structure of HBx is complicated and flexible due to the presence of a relatively long loop. We also subcloned and overexpressed truncated GLI1 successfully in *E. coli* and examined the evidence that binds HBx to GLI1. This study provides important clues for the structural identification of signal transduction pathways involving the HBx and GLI1 proteins.

Acknowledgements This study was supported for 2 years by Pusan National University Research Grant.

References

1. Arbuthnot, P., & Kew, M. (2001). Hepatitis B virus and hepatocellular carcinoma. *International Journal of Experimental Pathology, 82*(2), 77–100.
2. Murakami, S. (1999). Hepatitis B virus X protein: structure, function biology. *Intervirology, 42*(2–3), 82–99.
3. Murakami, S. (2001). Hepatitis B virus X protein: a multifunctional regulator. *Journal of Gastroenterology, 36*(10), 651–660.
4. Shirakata, Y., Kawada, M., Fujiki, Y., Sano, H., Oda, M., Yaginuma, K., et al. (1989). The x gene of hepatitis B virus induced growth stimulation and tumorigenic transformation of mouse NIH3T3 cells. *Japanese Journal of Cancer Research, 80*(7), 617–621.
5. Hohne, M., Schaefer, S., Scifer, M., Feitelson, M. A., Paul, D., & Gerlich, W. H. (1990). Malignant transformation of immortalized transgenic hepatocyte after transfection with hepatitis B virus DNA. *The EMBO Journal, 9*(4), 1137–1145.
6. Kim, C.-M., Koike, K., Saito, I., Miyamura, T., & Jay, G. (1991). HBx gene of hepatitis B virus induces liver cancer in transgenic mice. *Nature, 351*(6324), 317–320.
7. Yu, D. Y., Moon, H. B., Son, J. K., Jeong, S., Yu, S. L., Yoon, H., et al. (1999). Incidence of hepatocellular carcinoma in transgenic mice expressing the hepatitis B virus X-protein. *Journal of Hepatology, 31*(1), 123–132.
8. Billet, O., Grimber, G., Levrero, M., Seye, K. A., Briand, P., & Joulin, V. (1995). In vivo activity of the hepatitis B virus core promoter: tissue specificity and temporal regulation. *Journal of Virology, 69*(9), 5912–5916.
9. Terradillos, O., Billet, O., Renard, C. A., Levy, R., Molina, T., Briand, P., et al. (1997). The hepatitis B virus X gene potentiates c-myc-induced liver oncogenesis in transgenic mice. *Oncogene, 14*(4), 395–404.
10. Madden, C. R., Finegold, M. J., & Slagle, B. L. (2001). Hepatitis B virus X protein acts as a tumor promoter in development of diethylnitrosamine-induced preneoplastic lesions. *Journal of Virology, 75*(8), 3851–3858.
11. Su, F., & Schneider, R. J. (1997). Hepatitis B virus HBx protein sensitizes cells to apoptotic killing by tumor necrosis factor alpha. *Proceedings of the National Academy of Sciences of the United States of America, 94*(16), 8744–8749.
12. Takada, S., Shirakata, Y., Kaneniwa, N., & Koike, K. (1999). Association of hepatitis B virus X protein with mitochondria causes mitochondrial aggregation at the nuclear periphery, leading to cell death. *Oncogene, 18*(50), 6965–6973.
13. Lu, Y. W., & Chen, W. N. (2005). Human hepatitis B virus X protein induces apoptosis in HepG2 cells: role of BH3 domain. *Biochemical and Biophysical Research Communications, 338*(3), 1551–1556.
14. Kim, S., Kim, H.-Y., Lee, S., Kim, S. W., Sohn, S., Kim, K., et al. (2007). Hepatitis B virus X protein induces perinuclear mitochondrial clustering in microtubule- and dynein-dependent manners. *Journal of Virology, 81*(4), 1714–1726.
15. Ruizi, A. A. (1999). Gli proteins encode context-dependent positive and negative functions: implications for development and disease. *Development, 126*(14), 3205–3216.

16. Sasaki, H., Hui, C., Nakafuku, M., & Kondoh, H. (1997). A binding site for Gli proteins is essential for HNF-3beta floor plate enhancer activity in transgenics and can respond to Shh in vitro. *Development, 124*(7), 1313–1322.
17. Liu, C. Z., Yang, J. T., Yoon, J. W., Villavicencio, E., Pfendler, K., Walterhouse, D., et al. (1998). Characterization of the promoter region and genomic organization of GLI, a member of the Sonic hedgehog-Patched signaling pathway. *Gene, 209*(1–2), 1–11.
18. Callahan, C. A., et al. (2004). MIM/BEG4, a Sonic hedgehog-responsive gene that potentiates Gli-dependent transcription. *Genes & Development, 18*(22), 2724–2729.
19. Lo, S. J., Chien, M. L., & Lee, Y. H. (1988). Characteristics of the X gene of hepatitis B virus. *Virology, 167*(1), 289–292.
20. Kinzler, K. W., Ruppert, J. M., Bigner, S. H., & Vogelstein, B. (1988). The Gli gene is a member of the Kruppel family of zinc finger proteins. *Nature, 332*(6162), 371–374.
21. Kinzler, K. W., & Vogelstein, B. (1990). The Gli gene encodes a nuclear protein which binds specific sequences in the human genome. *Molecular and Cellular Biology, 10*(2), 634–642.
22. Gupta, A., Mal, T. K., Jayasuryan, N., & Chauhan, V. S. (1995). Assignment of disulphide bonds in the X protein (HBx) of hepatitis B virus. *Biochemical and Biophysical Research Communications, 212*(3), 919–924.